Nanoscale

Accepted Manuscript

This article can be cited before page numbers have been issued, to do this please use: A. Gallardo, Y. Pereyra, E. Martinez-Campos, C. Garcia, D. Acitores, I. Casado-Losada, M. A. Gómez, H. Reinecke, G. Ellis, D. Acevedo, J. Rodriguez Hernandez and H. J. Salavagione, *Nanoscale*, 2017, DOI: 10.1039/C7NR03204H.

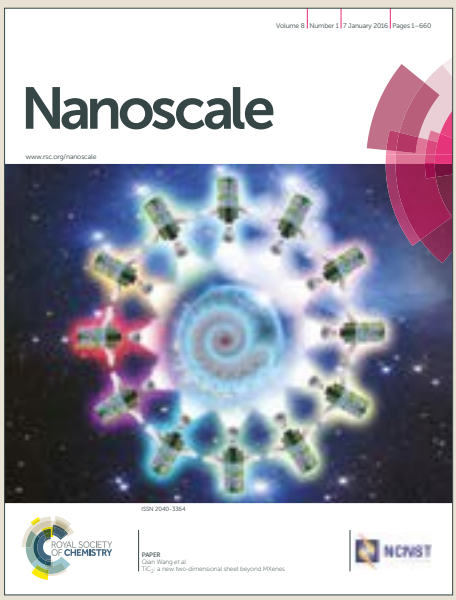

ROYAL SOCIETY OF CHEMISTRY

rsc.li/nanoscale

ROYAL SOCIETY OF CHEMISTRY View Article Online
DOI: 10.1039/C7NR03204H

Journal Name

COMMUNICATION

Facile One-pot Exfoliation and Integration of 2D Layered Materials by Dispersion in a Photocurable Polymer Precursor

Received 00th January 20xx,
Accepted 00th January 20xx

DOI: 10.1039/x0xx00000x

www.rsc.org/

Alberto Gallardo,[a] Yanina Pereyra,[b] Enrique Martínez-Campos,[c] Carolina García,[d] David Acitores,[c] Isabel Casado-Losada,[c] Marián A. Gómez-Fatou,[e] Helmut Reinecke,[a] Gary Ellis,[e] Diego Acevedo,[b] Juan Rodríguez-Hernández,[f] Horacio J. Salavagione[e,*]

Efficient exfoliation of graphene and related materials (GRM) and fast and inexpensive integration/assembly are crucial to fulfil their full potential. A high degree of exfoliation in organic media can be achieved with high boiling point liquids that usually leave residues after drying, which is a handicap for many applications. Here, the effective exfoliation and dispersion of GRM in a vinyl monomer, which is subsequently converted to a functional polymer by photopolymerization, is reported. Nanocomposite membranes and three-dimensional objects are produced by the photo-curing process and stereolithography 3D printing, respectively.

Layered 2D materials, such as graphene (Gr) and molybdenum sulfide (MoS_2), have been attracting huge interest due to unique properties that make them important candidates for many applications.[1-3] The combination of GRM with polymers is especially interesting since the product joins the superlative properties of GRM with those of polymers such as lightweight, flexibility, easy-processing into different shapes and chemical versatility. In this process, we distinguish three main steps, directly related to advances in technological applications: i) the large-scale production of GRM with the same properties as those determined in suspended monolayers, ii) the need for functionalization or modification to improve their interaction with host polymers, and iii) the production process.

With respect to the first step, different methods have been proposed for the mass production of GRM materials[4-7]. Liquid phase exfoliation of GRM is envisaged as one of the preferred methods as it permits large-scale preparation of single or few-layer nanomaterial with different lateral dimensions and structural integrity.[8-11] It has been demonstrated that the best solvents for dispersing GRM are those with similar surface energies as the bulk crystal, [12] However, these organic solvents (N-Methyl-2-Pyrrolidone -NMP, N,N'-dimethylformamide-DMF) display high boiling points and are difficult to eliminate thus leaving residues after evaporation,[12] thereby hampering their final use in technological applications. In addition, toxicity of NMP residues is also a critical issue from both health and environmental points of view[13] in view of their exploitation for biorelated purposes. Water dispersion of GRM has been also described, but in most cases, it requires additives or surfactants, [14-18] introducing additional components that limit effective upscaling.

Regarding the second step, it has been broadly demonstrated that efficient synergy by combination of GRM with polymeric materials leading to superior properties is only achieved when the compatibility between materials is substantially improved, by means of a strong nanoparticle/polymer interface.[19, 20] To ensure robust interfacial interactions, the GRM must be chemically functionalized with specific moieties with high affinity for the matrix,[21] which usually requires several chemical steps with purification protocols that diminish their attractiveness for industrial production.

With respect to the fabrication process, undoubtedly additive manufacturing (AM) is a leading and disruptive technology for the preparation of polymeric membranes. Among the different AM alternatives, stereolithography (SLA) 3D printing holds great potential for the production of complex structures. Well-established and widely used with polymers due to high precision (resolution: z axis < 20 μm, xy < 40-50 μm), that is cost effective with customized geometry,[22] the integration of nanomaterials into 3D printing processing opens a broad spectrum of possibilities and displays huge potential for the preparation of advanced multifunctional materials.[23] In fact, a

[a] Polymer Functionalization Group, Department of Applied Macromolecular Chemistry, Institute of Polymer Science and Technology (ICTP-CSIC), Juan de la Cierva 3, 28006 Madrid, Spain
[b] Department of Chemistry, University of Río Cuarto and CONICET. Ruta 36 km 601, Río Cuarto, Córdoba, 5800, Argentina.
[c] Institute of Biofunctional Studies (IEB), Tissue Engineering Group, (UCM), Associated Unit to the Institute of Polymer Science and Technology (ICTP-CSIC), Polymer Functionalization Group. Paseo de Juan XXIII 1, 28040 Madrid, Spain.
[d] Service of Characterization of Polymers, Institute of Polymer Science and Technology (ICTP-CSIC)- Juan de la Cierva 3, 28006, Madrid, Spain
[e] Department of Polymer Physics, Elastomers and Energy Applications, Institute of Polymer Science and Technology (ICTP-CSIC), Juan de la Cierva 3, 28006 Madrid, Spain
[f] Department of Chemistry and Properties of Polymers, Institute of Polymer Science and Technology (ICTP-CSIC), Juan de la Cierva 3, 28006, Madrid, Spain
Electronic Supplementary Information (ESI) available: Full experimental details, physic-chemical properties of monomers, additional characterization of L2DM dispersions and hydrogel membranes and cell culture studies.
See DOI: 10.1039/x0xx00000x

printable hydrogel composed of methacrylated chitosan as the host polymer and graphene derivatives that could be processed by 3D printing, has been very recently prepared.[24] However, in this case the preparation of the composites involved several steps.

In the present communication we describe a facile method to produce membranes of GRM-based polymeric nanocomposites by simple dispersion of graphene in a monomeric precursor with appropriate physico-chemical properties for liquid exfoliation, vinylpyrrolidone (VP), and subsequent photocuring giving polyvinylpyrrolidone (PVP), a non-ionic amphiphilic and biocompatible polymer capable to form hydrogels for biomedical applications like cell manipulation. [25]

One of the best solvents for liquid exfoliation of 2D materials is NMP and its effectiveness has been associated with properties like the surface energy and the Hildebrand parameter,[9] which is related to the total cohesive energy density of the solvents, and is divided in the dispersion (δ_D), polar (δ_P) and H-bonding (δ_H) contributions to dispersion according to the Hansen solubility parameters. The reported values of these parameters for VP are similar to that for NMP and closer to those for graphene and MoS_2 (**Figure S1**). Very stable dispersions of GRM in VP were generated by applying ultrasound treatment to powdered graphite or MoS_2, followed by centrifugation to remove heavy aggregates (**Figure 1**). To maximize the amount of dispersed graphene, parameters such as initial graphite concentration (C_i), ultrasonication time (S_t) and type (pulsed, $S_{t,p}$ or continue, $S_{t,c}$) and centrifugation speed (V_c) were investigated. The final concentration of dispersed particles (C_{Gr}) was calculated from UV-Visible spectroscopy via the Lambert-Beer equation, using experimentally determined molar extinction coefficients at 660 nm of 1880 $L.g^{-1}.m^{-1}$, in the order of that reported for NMP.[12] The effect of each experimental parameter on the concentration of dispersed graphene particles is presented in Figure 1. As expected the concentration of dispersed graphene increased with both C_i and S_t applied, the effect being much greater in the case of $S_{t,c.}$(see more details in ESI). The maximum concentration achieved (0.4 $mg.mL^{-1}$, see table S2) may not be sufficient for some applications, but it may be increased by further variations in the experimental conditions or by applying already reported procedures.[16, 26]

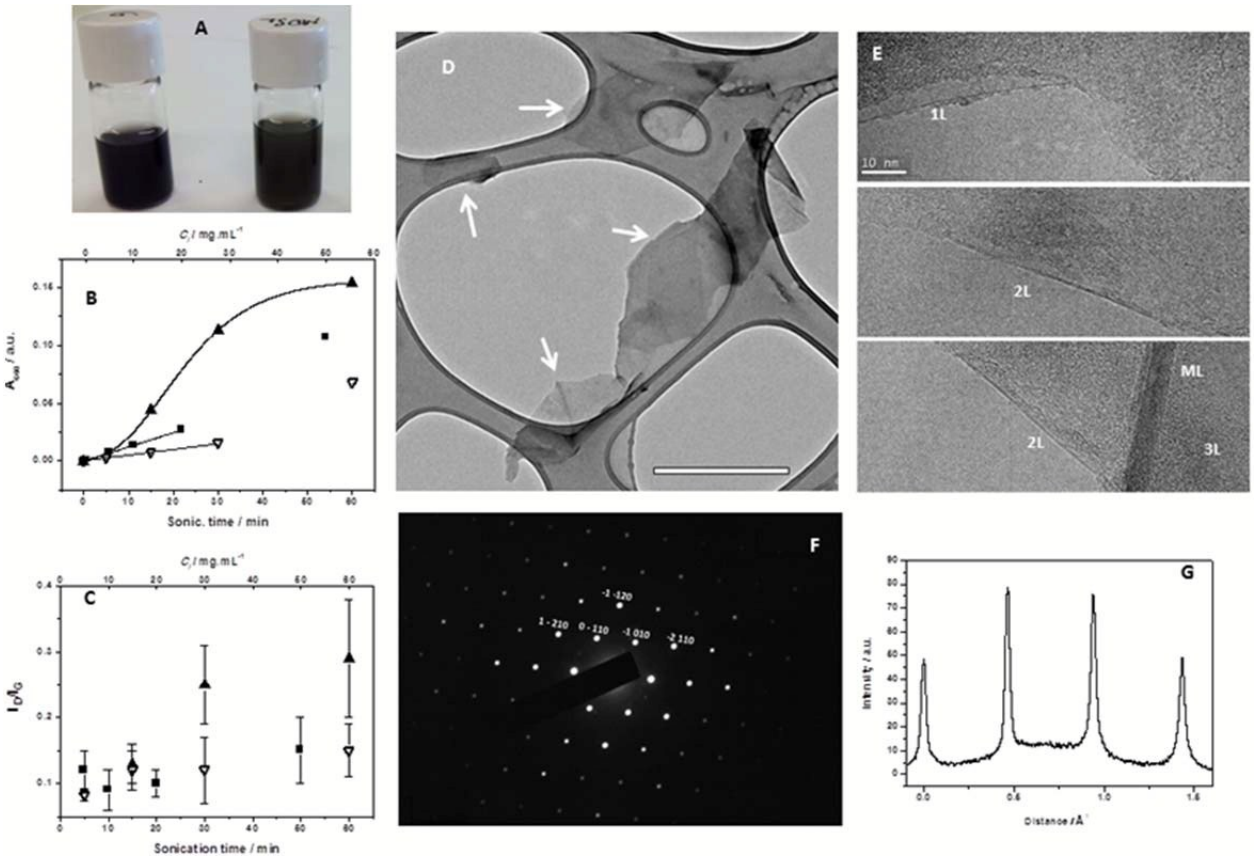

Figure 1. Characterization of GRM dispersed in VP. (A) Photograph of Gr (Left) and MoS_2 (right) dispersions after one month storage. (B) Variation of the amount of graphene dispersed in VP under different experimental conditions, obtained from absorption spectra. Squares represent C_i (top *x*-axis), while hollow and full triangles correspond to $S_{t,p}$ and $S_{t,c}$, respectively (bottom *x*-axis). Note that the effect of C_i is linearly adjusted by $[C_{Gr}] = 1{,}28 \times 10^{-3}\,[C_i]$ up to C_i = 20 $mg.mL^{-1}$; the influence of $S_{t,p}$ also follows a linear relationship of $[C_{Gr}] = 5 \times 10^{-4}\,[S_{t,p}]$, up to $S_{t,p}$ = 30 min, while the effect of $S_{t,c}$ is described by $[C_G] = 0.16 \cdot \exp(-5 \cdot \exp[-0.1[S_{t,c}]])$. (C) Dependence of the quality of flakes, determined by the I_D/I_G Raman ratio, for samples prepared under different experimental conditions (symbols code is the same as in B). (D) Typical TEM image showing graphene flakes of different lateral dimensions (scale bar corresponds to 0.5 μm), (E) HRTEM of flakes with different thickness ranging from monolayer to multilayer, (F) electron diffraction pattern of a monolayer, with the peaks labelled by Miller–Bravais indices and (G) diffracted intensity taken along the 1–210 to –2110 axis for the pattern in (F).

View Article Online
DOI: 10.1039/C7NR03204H

Journal Name

COMMUNICATION

We also analyzed the quality of the dispersed material by Raman spectroscopy. While all samples display the characteristic bands of graphene, i.e. the G band appearing around 1580 cm^{-1}, the second order 2D band at around 2700 cm^{-1} and the disorder-induced D band at 1350 cm^{-1} (Figure S3), the relationship of peak intensity of D with respect to the G band depends on the experimental conditions used to exfoliate graphite (Figure 1D). While the D/G intensity ratio seems to be independent of both C_i and $S_{t,p}$, it clearly increases as $S_{t,c}$ increases, again due to the hot spots where very high temperatures and pressures are generated in the cavitation waves. Further analysis of the Raman I_D/I_G intensity ratio for graphene in VP prepared under different experimental conditions reveals that other quality parameters are also generally affected when continues ultrasound wave is applied (Figure S4). The mean in-plane crystallite size, L_a, the distance between defects, L_D, and the density of defects, n_D, calculated with the appropriate equations from literature;[27, 28] also highlight the differences between the quality of the materials depending on the type of ultrasound treatment. The values obtained for fifteen minutes of continuous ultrasound are 138 $\pm$ 37 nm, 33 $\pm$ 4 nm and 3.4 x $10^{10} \pm$ 7.3 x 10^9 cm^{-2} for L_a, L_D and n_D, respectively, which are very similar to values obtained for graphene dispersed in NMP under the same conditions.[13] Considering the results presented, we selected the samples prepared under these conditions for further studies.

The dimensions and thicknesses of the dispersed flakes were analyzed by TEM. In the case of graphene a good concentration of 2D laminates is observed with some logical heterogeneity in both the lateral dimensions of the flakes and their thickness (Figure 1D and S5). Statistical analysis (of at least 40 flakes) reveals that the average length and width of the flakes are around 783 $\pm$ 220 nm and 337 $\pm$77 nm, respectively. The average length of flakes was also calculated using a recently reported expression that relates the full-width at half-maximum (FWHM) of the G band (Γ_G) with the mean size of flakes (<L>).[29] In this sample the mean size obtained was 793 $\pm$ 103 nm, in good agreement with TEM values. In addition, <L> has been observed to depend on the experimental conditions. It markedly decreases with $S_{t,c}$, is independent of $S_{t,p}$ and increases with a rate of 30 $nm.mg^{-1}$ with C_i for $C_i \leq$ 20 $mg.mL^{-1}$ (Figure S6). HRTEM allows the determination of the number of layers at the edge by counting the number of folds. Figure 1E shows HRTEM images of a flake with well-defined edges, where isolated single-layer and bilayer graphene are observed along with zones where bilayer, three-layer and multilayer coexist. Statistical inspection of these edges (40 flakes analyzed) suggests that around 15% of the total number of flakes are monolayer and over 73% of them are few-layer, which is slightly lower than values observed with NMP.[12] Normal-incidence electron diffraction pattern of the monolayer of Figure 1F shows the typical six-fold symmetry of graphene and the peaks are labeled with the Miller–Bravais (*hkil*) indices. Diffracted intensity taken along the 1–210 to 2–110 axis for the pattern in Figure 1F demonstrate that the intensity of the inner spots is higher than that of the outer ones (Figure 1G), which corresponds to a single-layer,[12] confirming the relation between the number of folds at the edges and the number of layers of the flake. TEM characterization of the MoS_2 flakes dispersed in VP (C_i = 20 $mg.mL^{-1}$; $S_{t,c}$ = 30 min; V_c = 7 kr.p.m.) is described in the ESI (Figure S5 D-F).

The VP-dispersed graphene and MoS_2 were photocured using a previously optimized formulation,[25] in the presence of potassium sulfopropylmethacrylate (17 mol.% with respect to VP), ethylene glycol dimethacrylate (2 mol.%), 3,3'-(propyl)-di-1-vinyl-2-pyrrolidone (0.1 mol.%) and water as solvent (Scheme S1. See full details in experimental section). A summary of the hydrogel types prepared is given in **Table S2**.

An image of the hydrogel film, hydrated at equilibrium, formed from a dispersion of 0.12 $mg.mL^{-1}$ of graphene is shown in **Figure 2.** A TEM image of a membrane containing 0.024 wt. % of graphene laminates is shown in Figure 2B, where irregularly shaped sheets with lateral size of a few hundred nanometers are seen. Folded edges are also observed as darker lines, most of them composed of few-layer graphene. A representative image of these edges is shown in Figure S8, in this case four layers are observed with a distance between the outer laminates of around 6 nm, which confirms the presence of polymer between graphene laminates (d-spacing in graphite is 0.34 nm).

The hydrogel membranes have been characterized by a pool of techniques in order to analyze the effect of the GRM on their bulk and surface properties. Swelling of hydrogel nanocomposites, obtained by gravimetry, was similar at ~82-83.5% (wet weight-dry weight)/wet weight. The mesh size, determined from the swelling data [30] slightly increase for the nanocomposites, suggesting a small decrease on the degree of crosslinking. Furthermore, the kinetics of swelling are very similar for all samples (data not shown), in spite of the water repulsion ability of graphene.[31] The load of GRM exerted a slight influence on the mechanical properties of the hydrogels (Table S3 and Figure S8). Independently of the GRM nature, a small decrease in the modulus, as obtained from compression tests, was observed (it ranged between 0.4 and 0.9 MPa). Deformation at break ranged between 80 – 90 % with similar values for the nanocomposite hydrogels as for the neat polymer hydrogel (Table S3). The absence of reinforcing effect

with the incorporation of the nanomaterials, which does occur in other hydrogel systems,[24, 32] can be understood considering the low final concentration of the GRM in the membranes, as observed for other graphene- based polymer nanocomposites.[33] Firstly, the high capability to incorporate water of the hydrogels led to materials with very high content of water, differently to other hydrogels.[24] Secondly, in the final polymerization formulation, 50-60 wt. % corresponds to VP with dispersed GRM. In this sense, more experiments are currently underway in order to increase the concentration of GRM.

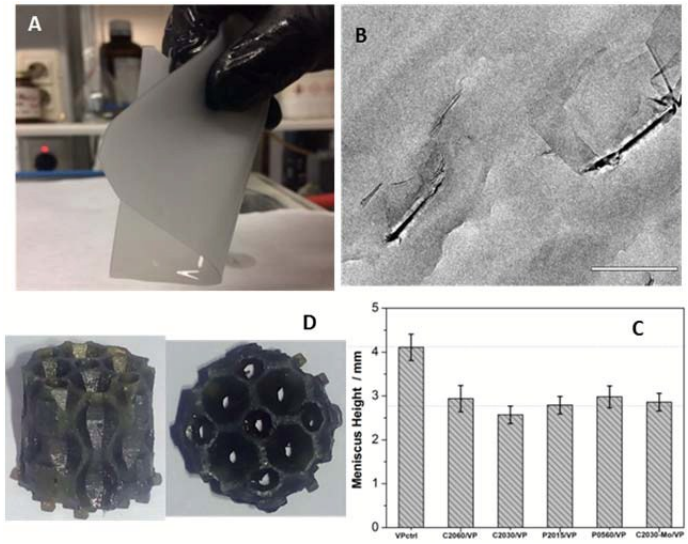

Figure 2. (A) Photograph of a hydrogel nanocomposite film after photocuring; (B) TEM image showing the dispersion of the flakes within the polymer hydrogel. Scale bar corresponds to 200 nm. (C) Capillary rise (meniscus height) for the hydrogels nanocomposites in water as a function of the surface chemical composition. (D) Side and top photographic views of a 3D object with a diameter of 13.4 mm, prepared by 3D photocuring.

The surface wettability was measured by using the capillary rise approach[34] that can be directly related to the dynamic contact angle[35, 36](see more details in ESI). The capillary rise values (measured in cm) obtained for the different hydrogels have been represented in Figure 2C for the different graphene/hydrogel (VP-Gr) and MoS_2/hydrogel (VP- MoS_2) materials. Interestingly, whereas the hydrogel employed as a control presented a meniscus height above 4 cm, the meniscus heights obtained for the nanocomposite hydrogels were between 2.5 and 3.2 cm. Thus, we can suggest that the incorporation of nanofillers, even at low concentration, produced measurable changes in the surface wettability.

One of the most interesting aspects of photopolymerizable hydrogel precursors are their possible use in AM to create 3D objects. As a proof of concept, we have used stereolithography (SLA) to fabricate a 3D scaffold using a monomer mixture of VP dispersed graphene and poly(ethylenglycol dimethacrylate), PEGDMA (average M_n = 550 g.mol^{-1}) in a volume ratio 1:1 (Figure 2D). By using the additive manufacturing methodology, the photopolymerization of precisely designed areas in a layer-by-layer approach permits the use of rather opaque solutions since the height of the layer can be limited to only a few microns. Thus, as depicted in Figure 2, in spite of the opacity of the monomer solution employed the formation of well-defined (micrometer resolution) and intricate geometries could be achieved.

VP-GRM based hydrogel membranes were used as cell culture platforms as soft-nanocomposites of polymeric gels and GRM-based nanoparticles, have demonstrated great potential for bio-applications.[37] Here, after an initial delay in the first days, cell aggregates over the surface were observed at 168 h (**Figure S10**). In the case of graphene, no significant differences were detected between samples, showing that cytocompatibility was not affected with the incorporation of the nanofiller. Metabolic evaluation also showed a similar level of activity on these samples (Figure S10). For cell detachment analysis, hydrogels were moved to a new 24-well tissue culture plate (TCP), inverting the hydrogel and bringing into contact the cell culture with the plastic surface for at least 4 hours. The hydrogels were removed and after 72 hours cell monolayers proliferated on the TCP without loss of viability, and optimal values of metabolic activity were achieved (**Figure 3**). No significant differences were found between detached cultures for the supports incorporating graphene. In the case of VP-MoS_2, a slight increase in the metabolic activity before and after transplantation was observed, in good agreement with other biological studies in molybdenum-based biomaterials.[17, 38-40] Finally, endothelial cells growing over VP-MoS_2 presented a more outstretched phenotype, in contrast with other hydrogels, were cells presented a rounded morphology (Fig. S10). This could represent a differential adhesion behavior over hydrogels surfaces, a fact that will be analyzed in future experiments.

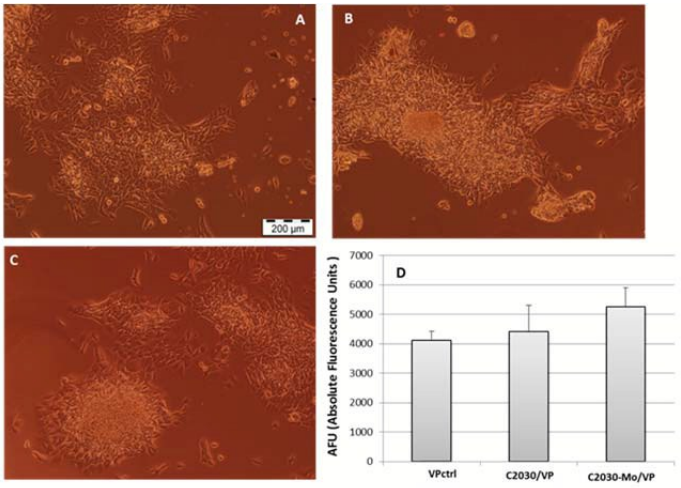

Figure 3. Evaluation of cell transplants (72h after detachment). Bright field images of (A) VP hydrogel with (B) graphene and (C) MoS_2. The scale bar in A applies to all images. (D) metabolic activity (Alamar Blue).

Conclusions

In conclusion, we have described a simple one-pot method to process graphene from graphite to the final product, in this

case hydrogel nanocomposites, by appropriately selecting the dispersion medium. Avoiding liquid solvents that are hard to remove and the simplicity of the protocol make it appealing for industrial scale-up. In addition, the combination of two families of materials (graphene or MoS_2 and a polymer hydrogel) with very different but complementary properties by means of such a facile method opens a wide range of possibilities for materials preparation and applications. The method reported in this communication can be extended to a broad scope of applications beyond bio-based ones as the many possible combinations between vinyl co-monomers open new opportunities for the preparation of diverse graphene-based copolymers with properties beyond hydrogels. Finally, the preliminary results described here on the integration of GRM into 3D printing processing have enormous potential implications for the preparation of advanced multifunctional materials.

Acknowledgements

This work was supported by MINECO (Spain, MAT2013-47898-C2-2-R, MAT2014-54231-C4-4-P, MAT2013-42957-R, MAT2016-78437-R) and FONCYT (Argentina, PICT-2716-2013)

Notes and references

1. F. Bonaccorso, A. Bartolotta, J. N. Coleman and C. Backes, *Advanced Materials*, 2016, **28**, 6136-6166.
2. Y. Chen, C. Tan, H. Zhang and L. Wang, *Chemical Society Reviews*, 2015, **44**, 2681-2701.
3. X. Zhang, L. Hou, A. Ciesielski and P. Samorì, *Advanced Energy Materials*, 2016, **6**, 1600671-n/a.
4. Y. L. Zhong, Z. Tian, G. P. Simon and D. Li, *Materials Today*, 2015, **18**, 73-78.
5. M. Yi and Z. Shen, *Journal of Materials Chemistry A*, 2015, **3**, 11700-11715.
6. K. R. Paton, E. Varrla, C. Backes, R. J. Smith, U. Khan, A. O'Neill, C. Boland, M. Lotya, O. M. Istrate, P. King, T. Higgins, S. Barwich, P. May, P. Puczkarski, I. Ahmed, M. Moebius, H. Pettersson, E. Long, J. Coelho, S. E. O'Brien, E. K. McGuire, B. M. Sanchez, G. S. Duesberg, N. McEvoy, T. J. Pennycook, C. Downing, A. Crossley, V. Nicolosi and J. N. Coleman, *Nat Mater*, 2014, **13**, 624-630.
7. D. Parviz, F. Irin, S. A. Shah, S. Das, C. B. Sweeney and M. J. Green, *Advanced Materials*, 2016, **28**, 8796-8818.
8. V. Nicolosi, M. Chhowalla, M. G. Kanatzidis, M. S. Strano and J. N. Coleman, *Science*, 2013, **340**.
9. J. N. Coleman, M. Lotya, A. O'Neill, S. D. Bergin, P. J. King, U. Khan, K. Young, A. Gaucher, S. De, R. J. Smith, I. V. Shvets, S. K. Arora, G. Stanton, H.-Y. Kim, K. Lee, G. T. Kim, G. S. Duesberg, T. Hallam, J. J. Boland, J. J. Wang, J. F. Donegan, J. C. Grunlan, G. Moriarty, A. Shmeliov, R. J. Nicholls, J. M. Perkins, E. M. Grieveson, K. Theuwissen, D. W. McComb, P. D. Nellist and V. Nicolosi, *Science*, 2011, **331**, 568-571.
10. H. Tao, Y. Zhang, Y. Gao, Z. Sun, C. Yan and J. Texter, *Physical Chemistry Chemical Physics*, 2017, **19**, 921-960.
11. D. McManus, S. Vranic, F. Withers, V. Sanchez-Romaguera, M. Macucci, H. Yang, R. Sorrentino, K. Parvez, S. K. Son, G. Iannaccone, K. Kostarelos, G. Fiori and C. Casiraghi, *Nat Nano*, 2017, **advance online publication**.
12. Y. Hernandez, V. Nicolosi, M. Lotya, F. M. Blighe, Z. Sun, S. De, I. T. McGovern, B. Holland, M. Byrne, Y. K. Gun'Ko, J. J. Boland, P. Niraj, G. Duesberg, S. Krishnamurthy, R. Goodhue, J. Hutchison, V. Scardaci, A. C. Ferrari and J. N. Coleman, *Nat Nano*, 2008, **3**, 563-568.
13. H. J. Salavagione, J. Sherwood, M. De bruyn, V. L. Budarin, G. J. Ellis, J. H. Clark and P. S. Shuttleworth, *Green Chemistry*, 2017, **19**, 2550-2560.
14. L. Guardia, M. J. Fernández-Merino, J. I. Paredes, P. Solís-Fernández, S. Villar-Rodil, A. Martínez-Alonso and J. M. D. Tascón, *Carbon*, 2011, **49**, 1653-1662.
15. A. Ciesielski and P. Samori, *Chemical Society Reviews*, 2014, **43**, 381-398.
16. M. Ayán-Varela, J. I. Paredes, L. Guardia, S. Villar-Rodil, J. M. Munuera, M. Díaz-González, C. Fernández-Sánchez, A. Martínez-Alonso and J. M. D. Tascón, *ACS Applied Materials & Interfaces*, 2015, **7**, 10293-10307.
17. J. I. Paredes, J. M. Munuera, S. Villar-Rodil, L. Guardia, M. Ayán-Varela, A. Pagán, S. D. Aznar-Cervantes, J. L. Cenis, A. Martínez-Alonso and J. M. D. Tascón, *ACS Applied Materials & Interfaces*, 2016, **8**, 27974-27986.
18. R. Jalili, S. Aminorroaya-Yamini, T. M. Benedetti, S. H. Aboutalebi, Y. Chao, G. G. Wallace and D. L. Officer, *Nanoscale*, 2016, **8**, 16862-16867.
19. H. J. Salavagione, G. Martínez and G. Ellis, *Macromolecular Rapid Communications*, 2011, **32**, 1771-1789.
20. M. Zhang, Y. Li, Z. Su and G. Wei, *Polymer Chemistry*, 2015, **6**, 6107-6124.
21. H. J. Salavagione, *Journal of Materials Chemistry A*, 2014, **2**, 1738.
22. X. Wang, M. Jiang, Z. Zhou, J. Gou and D. Hui, *Composites Part B: Engineering*, 2017, **110**, 442-458.
23. R. D. Farahani, M. Dubé and D. Therriault, *Advanced Materials*, 2016, **28**, 5794-5821.
24. S. Sayyar, S. Gambhir, J. Chung, D. L. Officer and G. G. Wallace, *Nanoscale*, 2017, **9**, 2038-2050.
25. I. Aranaz, E. Martinez-Campos, M. E. Nash, M. G. Tardajos, H. Reinecke, C. Elvira, V. Ramos, J. Luis Lopez-Lacomba and A. Gallardo, *Journal of Materials Chemistry B*, 2014, **2**, 3839-3848.
26. U. Khan, A. O'Neill, M. Lotya, S. De and J. N. Coleman, *Small*, 2010, **6**, 864-871.
27. L. G. Cançado, K. Takai, T. Enoki, M. Endo, Y. A. Kim, H. Mizusaki, A. Jorio, L. N. Coelho, R. Magalhães-Paniago and M. A. Pimenta, *Applied Physics Letters*, 2006, **88**, 163106.
28. L. G. Cançado, A. Jorio, E. H. M. Ferreira, F. Stavale, C. A. Achete, R. B. Capaz, M. V. O. Moutinho, A. Lombardo, T. S. Kulmala and A. C. Ferrari, *Nano Letters*, 2011, **11**, 3190-3196.
29. C. Backes, K. R. Paton, D. Hanlon, S. Yuan, M. I. Katsnelson, J. Houston, R. J. Smith, D. McCloskey, J. F. Donegan and J. N. Coleman, *Nanoscale*, 2016, **8**, 4311-4323.
30. D. A. Carr and N. A. Peppas, *Macromolecular Bioscience*, 2009, **9**, 497-505.

View Article Online
DOI: 10.1039/C7NR03204H

31. A. Flores, H. J. Salavagione, F. Ania, G. Martinez, G. Ellis and M. A. Gomez-Fatou, *Journal of Materials Chemistry C*, 2015, **3**, 1177-1180.
32. Y. Wang, S. Chen, L. Qiu, K. Wang, H. Wang, G. P. Simon and D. Li, *Advanced Functional Materials*, 2015, **25**, 126-133.
33. H. J. Salavagione, S. Quiles-Díaz, P. Enrique-Jimenez, G. Martínez, F. Ania, A. Flores and M. A. Gómez-Fatou, *Macromolecules*, 2016, **49**, 4948-4956.
34. D. Y. Kwok, C. J. Budziak and A. W. Neumann, *Journal of Colloid and Interface Science*, 1995, **173**, 143-150.
35. D. Quéré and J.-M. Di Meglio, *Advances in Colloid and Interface Science*, 1994, **48**, 141-150.
36. Y. Yuan and T. R. Lee, in *Surface Science Techniques*, eds. G. Bracco and B. Holst, Springer Berlin Heidelberg, 2013, vol. 51, ch. 1, pp. 3-34.
37. S. Bhattacharya and S. K. Samanta, *Chemical Reviews*, 2016, **116**, 11967-12028.
38. A. M. Ribeiro, T. H. S. Flores-Sahagun and R. C. Paredes, *J Mater Sci*, 2016, **51**, 2806-2816.
39. J. H. Appel, D. O. Li, J. D. Podlevsky, A. Debnath, A. A. Green, Q. H. Wang and J. Chae, *ACS Biomaterials Science & Engineering*, 2016, **2**, 361-367.
40. M. Ayán-Varela, Ó. Pérez-Vidal, J. I. Paredes, J. M. Munuera, S. Villar-Rodil, M. Díaz-González, C. Fernández-Sánchez, V. S. Silva, M. Cicuéndez, M. Vila, A. Martínez-Alonso and J. M. D. Tascón, *ACS Applied Materials & Interfaces*, 2017, **9**, 2835-2845.